ACS APPLIED MATERIALS & INTERFACES

Research Article

www.acsami.org

Fine Tuning of Nanocrystal and Pore Sizes of TiO_2 Submicrospheres toward High Performance Dye-Sensitized Solar Cells

Zhao-Qian Li,[†] Yong Ding,[†] Li-E Mo,[†] Lin-Hua Hu,[*,†] Ji-Huai Wu,[‡] and Song-Yuan Dai[*,§,†]

[†]Key Laboratory of Novel Thin-Film Solar Cells, Institute of Applied Technology, Hefei Institutes of Physical Science, Chinese Academy of Sciences, Hefei, Anhui 230031, P. R. China

[‡]Institute of Materials Physical Chemistry, Huaqiao University, Quanzhou 362021, P. R. China

[§]Beijing Key Laboratory of Novel Thin-Film Solar Cells, North China Electric Power University, Beijing 102206, P. R. China

Supporting Information

ABSTRACT: In general, the properties and performance of mesoporous TiO_2 are greatly dependent on its crystal size, crystallinity, porosity, surface area, and morphology; in this regard, design and fine-tuning the crystal and pore sizes of the TiO_2 submicrospheres and investigating the effect of these factors on the properties and photoelectric performance of dye-sensitized solar cells (DSSCs) is essential. In this work, uniform TiO_2 submicrospheres were synthesized by a two-step procedure containing hydrolysis and solvothermal process. The crystal and pore sizes of the TiO_2 submicrospheres were fine-tuned and controlled in a narrow range by adjusting the quantity of NH_4OH during the solvothermal process. The effect of crystal and pore size of TiO_2 submicrosphere on the performance of the DSSCs and their properties including dye-loading capacity, light scattering effect, power conversion efficiency (PCE), incident photon-to-electron conversion efficiencies (IPCEs), and electron recombination were compared and analyzed. The results show that increasing pore size plays a more significant role in improving the dye-loading capacity and PCE than increasing surface area, and an overall PCE value of 8.62% was obtained for the device with a 7.0 μm film thickness based on the TiO_2 submicrospheres treated with 0.6 mL of NH_4OH. Finally, the best TiO_2 submicrosphere based photoanode film was optimized by $TiCl_4$ treatment, and increasing film thickness and a remarkable PCE up to 11.11% were achieved.

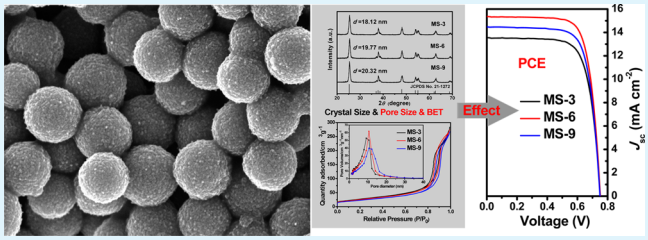

KEYWORDS: *mesoporous materials, TiO_2, submicrospheres, pore sizes, dye-sensitized solar cell*

1. INTRODUCTION

Anatase titanium dioxide (TiO_2) is one of the most widely investigated materials for many promising applications in environmental and energy areas ranging from photocatalysis,[1−4] to lithium ion batteries,[5−9] and solar cells.[9−18] Among all the reported TiO_2 micro/nanostructures, including nanoparticles,[19,20] nanotubes,[21−23] nanowires,[24,25] and submicro/microspheres,[7,13,26−29] mesoporous TiO_2 microspheres with unique microstructure and superior properties, such as large surface area and light scattering effect, have proved to be excellent candidates for these applications, especially in dye-sensitized solar cells (DSSCs). As an important part of DSSC, high BET surface area and dye-loading capacity, fast electron transport, and better light scattering for light harvesting are regarded as the premise for the success of the photoanode film.[13,26,27,30−32] In general, the properties and performance of mesoporous TiO_2 are greatly dependent on its crystal size, crystallinity, porosity, surface area, morphology, and composition;[19,33−36] in this regard, tuning the nano/microstructure of TiO_2 materials to optimize the photoanode film seems to be a promising way to obtain the DSSCs with high power conversion efficiency (PCE). Up to now, many efforts have been devoted to design and optimize the photoanode film, e.g., $TiCl_4$ post-treatment,[13,26,37] optimization of TiO_2 nanocrystal size,[35,36,38] construction of 1D−3D structures,[39] use of submicro/microsized spheres,[20,28,40] use of hollow[31,32] and hierarchical structured[3,41] TiO_2, or adoption of ZnO[42] and SnO_2[43] as photoanode. Because the crystal size and pore diameters have a profound and direct effect on the dye-loading, electron transport, collection, and recombination properties of DSSCs, they have received tremendous interest, and the results have considerably boosted the performance of DSSCs,[19,26,35,36] whereas present studies about microstructures, e.g., crystal size and pore size of the TiO_2 materials, mainly focus on the TiO_2 nanoparticle based DSSCs. As efficient and promising photoanode materials, studies about TiO_2 microspheres are still very rare. Only Cheng's group investigated the effect of TiO_2 bead diameter and pore sizes on the efficiency of DSSCs[26,44] and TiO_2 bead pore size on the performance of cobalt electrolyte based DSSCs,[45] and Grätzel's group researched the pore sizes and porosities of TiO_2 beads on the mass transport

Received: June 17, 2015
Accepted: September 22, 2015
Published: September 22, 2015

DOI: 10.1021/acsami.5b06556
ACS Appl. Mater. Interfaces 2015, 7, 22277−22283

properties of cobalt based redox couples in DSSC using YD2-o-C8 porphyrin dye as sensitizer.[13]

In recent years, a type of mesoporous TiO_2 sphere composed of anatase nanocrystals which was first reported by Cheng's group has received considerable attention and exhibited excellent performance in the photovoltaic field.[13,20,26,27,44,45] In 2014, Grätzel's group adopted these mesoporous TiO_2 spheres as photoanode to improve the mass transport of cobalt redox couples in DSSCs, and achieved an efficiency up to 11.4%,[13] which is the record PCE value for the TiO_2 sphere based DSSC. Thus, we could expect that this type of TiO_2 sphere will be a potential photoanode material, and undoubtedly, there will be photovoltaic devices based on this type of TiO_2 spheres achieving much higher power conversion efficiency (PCE) further. In the past two decades, the I_3^-/I^- redox mediator has been the most widely used liquid electrolyte in DSSCs inasmuch as its long-term stability, fast dye regeneration, and slow recombination between generated electrons in TiO_2 and tri-iodide.[20,40,46−48] Until now, it is still the classic and most widely utilized electrolyte, and importantly, most reported work about DSSCs is based on the I_3^-/I^- redox electrolyte yet, whereas, research about the effect of mesoporous structure of TiO_2 spheres on the I_3^-/I^- redox based DSSCs is very rare. In 2009, Cheng et al.[44] synthesized TiO_2 beads with controllable surface and pore size, and investigated the effect of pore size on the performance of DSSCs using N719 dye as sensitizer and I_3^-/I^- redox as electrolyte, whereas, in their work, the pore and crystal size were controlled in a relatively wide range (pore size 14−22.6 nm; crystal size 12−16 nm). Finally, in a comparison with P25 paste, the optimized TiO_2 beads spheres shows superior photovoltaic property, and an efficiency of 7.2% was obtained. So, to better utilize and explore the potential of this type of TiO_2 sphere, fine-tuning the mesoscopic structure, such as crystal sizes and pore diameters of TiO_2 spheres, and investigating the effect of it on the properties of DSSCs, especially I_3^-/I^- redox based DSSCs, is still a very pressing need and has research and practical significance for fabricating photovoltaic devices with higher PCE. Inspired by this idea, in this work, mesoporous TiO_2 submicrospheres with the same diameters but different and fine-tuned crystal size and pore diameters, denoted as MS-3, MS-6, and MS-9, were synthesized. The effect of difference in crystal size and pore diameters of the three as-prepared TiO_2 submicrospheres on the performance of the DSSCs and their properties, including light scattering effect, dye-loading capacity, PCE, incident photon-to-electron conversion efficiencies (IPCEs), and electron recombination rate, were compared and analyzed. Besides, the sensitizer is also an important factor for the high efficiency DSSCs.[49] In recent years, C101 dye has exhibited excellent performance in the DSSC field since it was reported by Wang's group.[50] Here, we adopt C101 dye as sensitizer and expect it can generate a better power conversion efficiency. Finally, on the basis of our research results, using C101 dye as sensitizer, the TiO_2 submicrosphere based photoanode film which possesses the best performance was optimized, and a remarkable PCE up to 11.11% was achieved.

2. RESULTS AND DISCUSSION

TiO_2 submicrospheres (MSs) were synthesized according to a modified procedure containing hydrolysis and the subsequent solvothermal process. Fabrication details are given in the Experimental Section. Here, to keep the same sphere diameters, the synthesis of the three TiO_2 submicrospheres started from the same precursor. The final crystal and pore sizes, and morphologies, were fine-tuned and determined by adjusting the quantity of NH_4OH (28 wt %, 0.3, 0.6, and 0.9 mL) during the solvothermal treatment process. Figure 1 and Figure S1 show

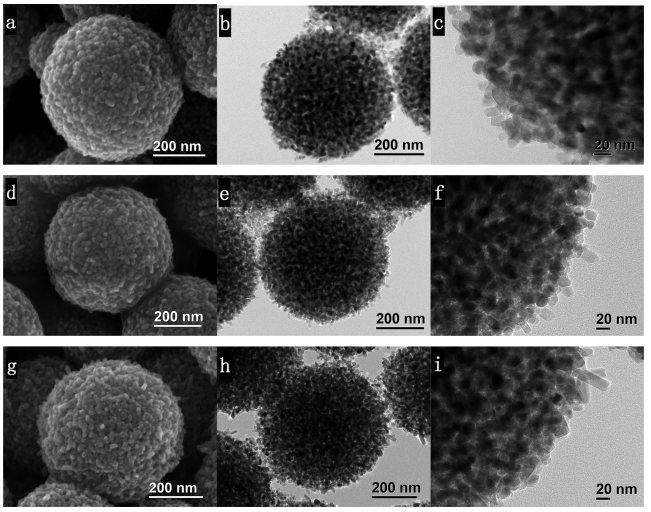

Figure 1. SEM and TEM images of the TiO_2 submicrospheres synthesized with the amount of NH_4OH of (a, b, and c) 0.3 mL (MS-3), (d, e, and f) 0.6 mL (MS-6), (g, h, and i) 0.9 mL (MS-9).

scanning electron microscopy (SEM) images of TiO_2 spheres with a diameter of ∼530 nm before and after solvothermal treatment. Upon solvothermal treating, the precursor spheres with a smooth surface (Figures S1a,b) transformed into uniform mesoporous submicrospheres consisted of interconnected TiO_2 nanocrystals (Figure S1c−e and Figure 1a,d,g). Transmission electron microscopy (TEM) images (Figure 1b,e,h) further confirmed their mesoporous structure. Importantly, from the TEM (Figure 1b,e,h) and high resolution TEM (HRTEM) (Figure 1c,f,i) images, we can see that, with increasing the quantity of NH_4OH (from 0.3, 0.6, to 0.9 mL), the sphere structure became more porous and the composed crystals grew larger.

Figure 2a shows the XRD patterns of the TiO_2 submicrospheres after sintering. All diffraction peaks can be assigned to

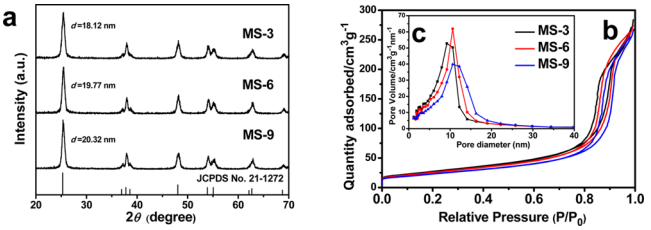

Figure 2. (a) XRD patterns, (b) nitrogen adsorption/desorption isotherms, and (c) the corresponding Barret−Joyner−Halenda (BJH) pore size distribution plots of the TiO_2 submicrospheres after sintering.

the anatase phase. With increasing the quantity of NH_4OH, the diffraction peak became sharper, suggesting a growth of the composed crystallites during solvothermal treatment. The average crystal sizes increase from 18.12, to 19.77, to 20.32 nm calculated by the Scherrer equation, which is in accordance with the HRTEM observation. Brunauer−Emmett−Teller

DOI: 10.1021/acsami.5b06556
ACS Appl. Mater. Interfaces 2015, 7, 22277−22283

(BET) surface areas and Barret–Joyner–Halenda (BJH) pore size distribution of the TiO_2 submicrospheres after sintering were analyzed by nitrogen adsorption–desorption. As shown in Figure 2b,c, increasing the quantity of NH_4OH leads to a decrease of surface area and pore volume but larger pore size. The larger pore size and decrease in surface area are in accordance with previous observation of more porous interior structures and larger crystal sizes by TEM analysis. The crystal and pore sizes, BET surface area, and pore volume of the as-prepared three TiO_2 submicrospheres are summarized in Table 1.

Table 1. TiO_2 Submicrosphere Properties after Sintering: Surface Area, Pore Size, Pore Volume, and Crystal Size

sample	surface area (m^2 g^{-1})	pore size (nm)	pore volume (cm^3 g^{-1})	D_{XRD} (nm)
MS-3	99.3	17.1	0.424	18.12
MS-6	93.8	17.9	0.419	19.77
MS-9	84.9	19.1	0.404	20.32

To investigate the light scattering behavior and dye-loading capacity, the three TiO_2 submicrosphere based films with the same thicknesses of ~7 μm was prepared via screen-printing method (Figure S2). Figure 3a shows the diffuse reflectance of the three TiO_2 submicrosphere based films measured using an integrating sphere. From Figure 3a, we can see that the three TiO_2 submicrosphere films all exhibit high diffuse reflection performance in the wavelength range from 400 to 800 nm because of the superior scattering effect in the visible light range induced by the comparable size of the mesoporous submicrospheres to the wavelength of visible light according to Mie theory. However, the difference of the three diffuse reflection spectra is that, with increasing the quantity of NH_4OH, namely, increasing crystal and pore sizes of submicrospheres, the diffuse reflection shows lower intensity. From Figure 3a, we can see that the light scattering capacity is in the order MS-3 > MS-6 > MS-9. A reasonable explanation may be that increasing the crystal and pore sizes of the submicrospheres will lead to more Rayleigh scattering of individual nanoparticles and lower the Mie scattering induced by larger submicro/micrometer spheres,[13] since here, the diffuse reflection of the submicrosphere based films mainly originates from Mie scattering.

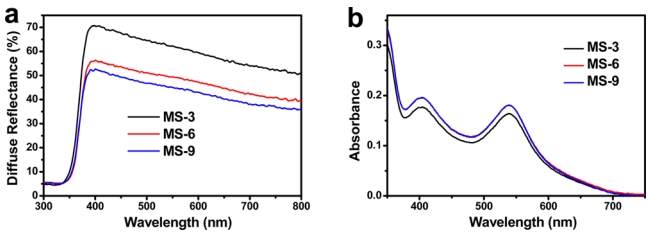

Figure 3. (a) Diffuse reflectance and (b) dye desorbed spectra from anode films based on MS-3, MS-6, and MS-9.

Dye loading capacity of the photoanode film is important for a DSSC because it significantly influences its photoelectron generation. Hence, C101 dye-loading of the three TiO_2 submicrospheres was measured by UV–vis spectroscopy after desorbing from a dye saturation adsorption film. From Figure 3b and Table 2, we can see that the dye-loading capacity is not proportional to the BET surface area. MS-6 and MS-9 show the similar dye-loading capacity at the same film thickness which is higher than MS-3 despite it possessing the highest BET surface area. Importantly, by comparing the effect of the BET surface area (from 99.3, to 93.8, to 84.9 m^2 g^{-1}) and pore size (from 17.1, to 17.9, to 19.1 nm) of MS-3, MS-6, and MS-9 on the dye-loading capacity (from 7.31, to 8.23, to 8.23 × 10^{-8} mol cm^{-2}), we can conclude that increasing pore size plays a more significant role in improving the dye-loading capacity than increasing surface area. Therefore, optimizing pore size of the TiO_2 submicrospheres seems to be an efficient way for more dye-loading and further improvement of PCE while keeping the BET surface area in a relatively high value (~80 m^2 g^{-1}). Here, it should be noted that BET surface area with a value of ~80 m^2 g^{-1} is already sufficient for the dye-loading in a DSSC, and up to now, the DSSC with the record PCE value is also based on the TiO_2 nanoparticles with a surface area of ~80 m^2 g^{-1}.[51] So, in this work, the poorer dye-loading capacity for MS-3 may mainly result from the smaller pore size distribution and less porosity.

To investigate the photovoltaic properties of the three TiO_2 submicrospheres, we fabricated complete solar cells using I_3^-/I^- redox liquid electrolyte and C101 dye as sensitizer. Figure 4a shows the J–V characteristics of pure MS-3, MS-6, and MS-9 based DSSCs without $TiCl_4$ or other treatment, and Table 2 summarizes the detailed photovoltaic parameters. With the same film thicknesses, the open circuit voltages show no obvious distinction among the three DSSCs; the highest PCE value (8.62%) for MS-6 comes from the highest photocurrent density (15.36 mA cm^{-2}) and a slightly large fill factor (74.71%). As illustrated above, the reason for the better performance of MS-6 than MS-3 and MS-9 might be ascribed to the higher dye-loading capacity combined with the superior

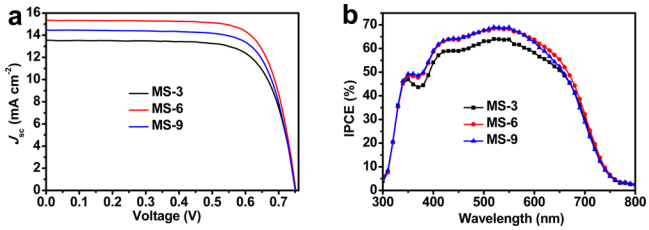

Figure 4. (a) Current density–voltage (J–V) characteristics under the illumination and (b) incident photon-to-electron conversion efficiencies (IPCEs) of MS-3, MS-6, and MS-9 based DSSCs.

Table 2. Comparison of the Photovoltaic Properties Measured under 1 Sun Illumination and Dye Adsorption Capacities for MS-3, MS-6, and MS-9 Based DSSCs

cell	thickness	dye-loading (10^{-8} mol cm^{-2})	J_{sc} (mA cm^{-2})	V_{oc} (V)	FF (%)	η (%)
MS-3	7.0 μm	7.31	13.55	0.750	73.09	7.43
MS-6	7.0 μm	8.23	15.36	0.751	74.71	8.62
MS-9	7.0 μm	8.23	14.48	0.749	74.00	8.03

DOI: 10.1021/acsami.5b06556
ACS Appl. Mater. Interfaces 2015, 7, 22277–22283

light scattering effect. Compared with MS-3, MS-6 shows a higher dye-loading capacity; at the same time, compared with MS-9, it shows a better light scattering property. As a result, when assembled to a DSSC, MS-6 could generate more photocurrent, leading to better photovoltaic performance. To demonstrate this, incident photon-to-electron conversion efficiencies (IPCEs) of the three submicrospheres based DSSCs were measured. As shown in Figure 4b, MS-6 and MS-9 show the higher IPCE than MS-3 almost in the entire wavelength range, and this should be induced by the higher dye-loading capacity for MS-6 and MS-9. While for the MS-6 and MS-9, because of the better light scattering effect, MS-6 exhibits a slightly higher IPCE compared with MS-9 in the wavelength region from 600 to 750 nm. Consequently, MS-6 shows the highest IPCE, namely, the highest photocurrent density, giving rise to the PCE up to 8.62%. Furthermore, to show the superior photovoltaic performances of the TiO_2 submicrospheres of this type, we also fabricated TiO_2 nanoparticle (NP) based DSSCs. As shown in Figure S3, NP based DSSCs generated much lower photocurrent density (12.28 mA cm^{-2}) than the three MS based DSSCs; as a result, only a PCE value of 6.88% was obtained.

In a DSSC, crystal and pore sizes of mesoporous TiO_2 have a great effect on the electron transport, recombination, and lifetime. Therefore, electrochemical impedance spectroscopy (EIS) of the three pure TiO_2 submicrosphere based DSSCs were measured at −0.73 V forward bias in the dark to investigate the dynamics of electron transport and recombination (Figure 5a), and the fitting data results are given in Table

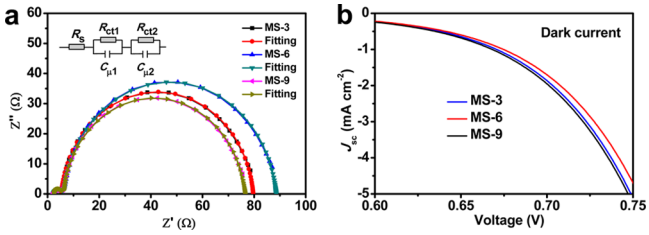

Figure 5. (a) Nyquist plots measured at −0.73 V forward bias and (b) current density−voltage (J−V) characteristics in the dark for MS-3, MS-6, and MS-9 based DSSCs.

Table 3. Electron Transfer and Recombination Resistance (R_{ct}) and Chemical Capacitance (C_μ) of MS-3, MS-6, and MS-9 Based DSSCs

cell	R_{ct} (Ω)	C_μ (μF)	$\tau_{n(EIS)}$ (ms)
MS-3	74.29	242.34	18.0
MS-6	82.24	235.57	19.4
MS-9	70.22	223.98	15.7

3. From Figure 5a and Table 3, we can see that increasing the quantity of NH_4OH resulted in a decrease of constant phase element (C_μ) value, but interestingly, the charge transfer and recombination resistance (R_{ct}) values are not in an order. MS-6 shows the larger R_{ct}, suggesting that it has a lower recombination rate. According to the equation $\tau_{n(EIS)} = R_{ct} \times C_\mu$,[11] the electron lifetimes are calculated to be 18.0, 19.4, and 15.7 ms for MS-3, MS-6, and MS-9, respectively. Clearly, MS-6 based DSSC shows the longest electron lifetime. In comparison with MS-3, the reason for the lower recombination rate and longer electron lifetime of the MS-6 might be ascribed to the less exposed BET surface area because less exposed surface area means that there will be less recombination for generated electrons occurring at the interface of TiO_2 nanocrystals/I_3^-/I^- electrolyte.[19,26] However, for the MS-9, despite it having a smaller BET surface area, the relatively larger pore size and higher porosity compared with MS-6 may allow more electron recombination to take place in the deeper interior of the micropheres since the higher porosity could facilitate the electrolyte diffusion into the sphere interior.[13,45] As a consequence, compared with MS-3 and MS-9, MS-6 shows the lower recombination rate leading to the longest electron lifetime, and thus, MS-6 based DSSC harvests the highest current density and PCE value. Furthermore, the dark current potential scans were also conducted to estimate the electron recombination of the three DSSCs. The results show that MS-6 based DSSC exhibits a lower dark current at the same potential above 0.6 V, which means that MS-6 has a lower electron recombination rate than MS-3 and MS-9 (Figure 5b). The dark J−V results are in good agreement with the EIS analysis.

Prior reports have demonstrated that $TiCl_4$ treatment and addition of a TiO_2 nanoparticle (NP) underlayer could improve the power conversion efficiency of the submicro/microsphere based DSSCs.[13,20,52,53] Hence, in this work, MS-6 based film was optimized by $TiCl_4$ treatment and addition of a 4.5 μm nanoparticle underlayer (Figure S2e) since it shows the best photovoltaic performance. Consequently, as shown in Figure 6a

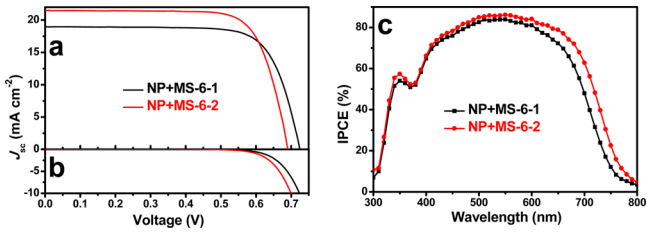

Figure 6. J−V characteristics (a) under the illumination and (b) in the dark and (c) incident photon-to-electron conversion efficiencies (IPCEs) of the optimized photoanode film based DSSCs with different film thicknesses.

Table 4. Photovoltaic Properties of DSSCs Based on Optimized MS-6 with Different Film Thicknesses

cell	thickness	J_{sc} (mA cm^{-2})	V_{oc} (V)	FF (%)	η (%)
NP + MS-6-1	4.5 + 7.1 μm	18.97	0.725	74.1	10.20
NP + MS-6-2	4.5 + 15.2 μm	21.53	0.691	74.7	11.11

and Table 4, the photocurrent increased to 18.97 mA cm^{-2}, and a PCE value of 10.20% was obtained. At the same time, thickness of the TiO_2 films plays a great role in the PCE inasmuch as it could increase the dye-loading and photocurrent density.[26,45] So, finally, by increasing the MS-6 film thickness from 7.1 to 15.2 μm, notwithstanding sacrificing the open circuit voltage (0.725 to 0.691 V), the photocurrent was significantly enhanced, leading to a big harvest of PCE, up to 11.11%. To prove the PCE results, IPCE values of both of the optimized DSSCs were measured. As shown in Figure 6c, in comparison with pure MS-6, the IPCEs of the two optimized DSSCs have a great increase. Importantly, we can see that, with

DOI: 10.1021/acsami.5b06556
ACS Appl. Mater. Interfaces 2015, 7, 22277−22283

increasing film thickness, the IPCE has a great enhancement, especially in longer wavelength range. We believe that this enhancement should be attributed to the superior light scattering effect of MS-6 compared to nanoparticles.

Generally, electron recombination occurring at the interface of $TiO_2/I_3^-/I^-$ electrolyte would result in a decrease of the V_{oc}.[26] In this work, for the optimized DSSCs, the decrease of V_{oc} could be demonstrated by the dark $J-V$ and EIS measurements. From Figure 6b, it is clear that the NP + MS-6-2 DSSCs exhibit a higher dark current at the same potential above 0.6 V, suggesting that NP + MS-6-2 DSSC has a higher electron recombination rate than that of NP+MS-6-1. EIS measurements were also conducted to analyze the recombination condition of both of the DSSCs. As shown in Figure 7 and

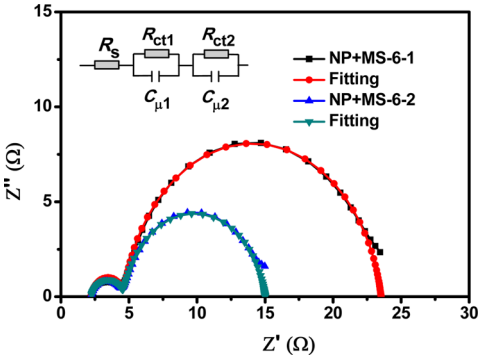

Figure 7. Nyquist plots of optimized MS-6 based DSSCs with different film thickness.

Table 5. Electron Transfer and Recombination Resistance (R_{ct}) and Chemical Capacitance (C_μ) of the Optimized MS-6 Based DSSCs with Different Film Thickness

cell	$TiCl_4$ treatment	R_{ct} (Ω)	C_μ (μF)	$\tau_{n(EIS)}$ (ms)
NP + MS-6-1	Y	18.91	1006.6	19.03
NP + MS-6-2	Y	10.41	1887.2	19.65

Table 5, NP + MS-6-2 DSSC shows smaller electron recombination resistance (R_{ct}) than NP + MS-6-1 DSSC, suggesting that the thicker film possesses much higher recombination rate, and this result is in good agreement with the dark $J-V$ measurement. Also, we can see that, accompanying the higher J_{sc} and recombination rate, the NP + MS-6-2 DSSC shows much larger C_μ value than NP + MS-6-1 DSSC. However, finally, according to the equation $\tau_{n(EIS)} = R_{ct} \times C_\mu$,[11] the electron lifetimes (τ_n's) of both of the DSSCs exhibit a similar value, calculated to be 19.03 and 19.65 ms for NP + MS-6-1 and NP + MS-6-2 DSSCs, respectively. From the τ_n results of the DSSCs with different film thicknesses, we could also conclude that the electron lifetime is an inherent property of a photoanode material, which could not be influenced by the film thickness. The slightly larger value for NP + MS-6-2 DSSC (19.65 ms) might be ascribed to the higher content ratio of TiO_2 MS than that in NP + MS-6-1 DSSC, since this type of TiO_2 MS possesses longer electron lifetime than TiO_2 nanoparticles.[28] Consequently, on the basis of the above analysis, we can see that increasing film thickness could improve the photocurrent density while enhancing the electron recombination rate, and finally leading to a lower V_{oc} value.

3. EXPERIMENTAL SECTION

Synthesis of Amorphous Spheres Precursor. All chemicals were used as received. Mesoporous TiO_2 submicrospheres were synthesized via a modified two-step process consisting of hydrolysis and subsequent solvothermal process based on the previously reported method.[3,13,54] In a typical synthesis, NH_4OH solution (28 wt %, 0.42 mL) and H_2O (0.91 mL) were added into a mixed solution containing 150 mL of ethanol and 100 mL of acetonitrile under vigorous stirring. Then, titanium isopropoxide (TIP, 5 mL) was promptly injected, and a milky suspension was formed within a few seconds. After continuous stirring for 6 h, the formed precipitate was centrifuged and washed with ethanol twice and dried at 60 °C.

Synthesis of Mesoporous TiO_2 Submicrospheres. The mesoporous TiO_2 microspheres with fine-tuned pore diameters and crystal sizes were synthesized by controlling the quantity of NH_4OH during the solvothermal process. Typically, dried precursor spheres (1.5 g) underwent solvothermal treatment in a mixture containing 40 mL of ethanol, 20 mL of water, and 0.6 mL of NH_4OH (28 wt %) at 160 °C for 16 h. The as-obtained solid product was collected by centrifugation, washed with ethanol twice, and dried at 60 °C, named MS-6. The other two products using 0.3 and 0.9 mL of NH_4OH (28 wt %) were synthesized under the same conditions, named as MS-3 and MS-9, respectively.

Assembly of Dye-Sensitized Solar Cells (DSSCs). For the photoanode, single layer films of interconnected TiO_2 particles were screen-printed on FTO-type TCO glass through a 34T meshsize screen. Different films were obtained by either varying the paste (either NP or TiO_2 submicrospheres paste) or by repeating the screen printing step several times. In this case the films were dried at 200 °C for 5 min between each print. In some cases, a NP underlayer was deposited by screen printed nanocrystalline paste. The resulting films were gradually heated in air to 510 °C and sintered at this temperature for 30 min before solar cell construction. A 300 μM portion of cheno-3a,7a-dihydroxy-5b-cholic acid was dissolved with an equimolar amount of C101 complex in a mixture of tert-butanol and acetonitrile solvent (1:1 by volume). After being washed by acetonitrile and dried in air, the overnight sensitized electrodes were sealed using a 60 μm thick Surlyn gasket, melted by heating with the Pt-modified TEC15 TCO counter electrode. The latter was prepared by spreading out a drop of 5 mM H_2PtCl_6 isopropyl alcohol solution onto the counter electrode before treating it at 450 °C for 30 min under air. A hole was introduced in the counter electrode by sand-blasting, allowing the internal space between the two electrodes to be filled with volatile electrolyte using a vacuum backfilling system, and then was sealed with a thin glass sheet. The electrolyte was composed of 1 M DMII, 50 mM LiI, 30 mM I_2, 0.5 M *tert*-butylpyridine, and 0.1 M GuNCS in a solvent mixture of 85% acetonitrile with 15% valeronitrile by volume.

Prior to measurements the cell was masked by a square black tape with a 5 × 5 mm^2 aperture.

Instruments. The morphology of the samples was investigated by scanning electron microscopy (FEI XL-30 SFEG coupled to a TLD) and transmission electron microscopy (TEM, JEM-200CX; JEOL). The X-ray diffraction (XRD) patterns were recorded using a Bruker-AXS microdiffractometer (model D5005) with Cu Kα radiation (λ = 1.5406 Å). The surface area, pore volume, and pore size were evaluated by using a Micromeritics (TriStar II 3020 V1.03, Micromeritics Instrument Corporation) nitrogen adsorption/desorption apparatus. Ultraviolet−visible (UV−vis) diffuse reflectance spectroscopy (DRS) and UV−vis absorption spectroscopy were performed using the UV−vis spectrophotometer (SOLID3700, Shimadzu Co. Ltd., Japan). Dye desorption measurements were carried out by detaching the C101 dye from the photoanode using a solution containing 0.5 mL of tetrabutylammonium hydroxide (10 wt % in water) and 10 mL of *N*,*N*-dimethylformamide (DMF). The amount of loaded dye was calculated from the UV−vis absorption spectrum of the resultant solution using $\varepsilon = 1.75 \times 10^4$ M^{-1} cm^{-1} as the molar extinction coefficient for C101 at 541 nm.

The ($J-V$) measurements were carried out on a Keithley model 2420 digital source meter controlled by Test point software under a

DOI: 10.1021/acsami.5b06556
ACS Appl. Mater. Interfaces 2015, 7, 22277−22283

xenon lamp (100 mW cm^{-2}). The IPCE values were confirmed as a function of wavelength from 300 to 800 nm (PV Measurements, Inc.) for DSSCs. The electrochemical impedance spectra (EIS) were recorded by a computer controlled potentiostat (Autolab 320, Metrohm, Switzer land) in a frequency range of 10 mHz to 1000 kHz applied in the dark.

4. CONCLUSIONS

In summary, TiO_2 submicrospheres were synthesized by a two-step procedure containing hydrolysis and solvothermal process. The crystal and pore sizes of the TiO_2 submicrospheres were fine-tuned and controlled in a narrow range by adjusting the quantity of NH_4OH during the solvothermal process. The crystal and pore size of TiO_2 submicrosphere has a significant effect on the properties of the DSSCs including light scattering effect, dye-loading capacity, PCE, IPCE, and electron recombination. The results show that TiO_2 submicrospheres treated with 0.6 mL of NH_4OH exhibit the best photovoltaic performance and an overall PCE value of 8.62% was obtained for the device with a 7.0 μm film thickness. Finally, the best TiO_2 submicrosphere (MS-6) based photoanode film was optimized by $TiCl_4$ treatment and increasing film thicknesses, and a remarkable PCE up to 11.11% was achieved.

■ ASSOCIATED CONTENT

Supporting Information

The Supporting Information is available free of charge on the ACS Publications website at DOI: 10.1021/acsami.5b06556.

Additional SEM images, cross-sectional and top view SEM images of TiO_2 films, and current density−voltage (J−V) characteristics of TiO_2 nanoparticles based DSSC (PDF)

■ AUTHOR INFORMATION

Corresponding Authors

*E-mail: solarhu@sina.com. Phone: +86 55165593222.
*E-mail: sydai@ipp.cas.cn. Phone: +86 1061772268.

Notes

The authors declare no competing financial interest.

■ ACKNOWLEDGMENTS

This work was supported by the National Natural Science Foundation of China (Nos. 21173228, U1205112, and 61204075), the National High Technology Research and Development Program of China (No. 2015AA050602), and the China Postdoctoral Science Foundation (No. 2014M551825).

■ REFERENCES

(1) Chen, X. B.; Liu, L.; Yu, P. Y.; Mao, S. S. Increasing Solar Absorption for Photocatalysis with Black Hydrogenated Titanium Dioxide Nanocrystals. *Science* **2011**, *331*, 746−750.

(2) Li, H.; Bian, Z.; Zhu, J.; Zhang, D.; Li, G.; Huo, Y.; Li, H.; Lu, Y. Mesoporous Titania Spheres with Tunable Chamber Stucture and Enhanced Photocatalytic Activity. *J. Am. Chem. Soc.* **2007**, *129*, 8406−8407.

(3) Pan, J. H.; Wang, X. Z.; Huang, Q.; Shen, C.; Koh, Z. Y.; Wang, Q.; Engel, A.; Bahnemann, D. W. Large-scale Synthesis of Urchin-like Mesoporous TiO_2 Hollow Spheres by Targeted Etching and Their Photoelectrochemical Properties. *Adv. Funct. Mater.* **2014**, *24*, 95−104.

(4) Zhao, Y.; Chen, Q.; Pan, F.; Li, H.; Xu, G. Q.; Chen, W. Uniform Mesoporous Anatase Hollow Spheres: An Unexpectedly Efficient Fabrication Process and Enhanced Performance in Photocatalytic Hydrogen Evolution. *Chem. - Eur. J.* **2014**, *20*, 1−7.

(5) Ren, H.; Yu, R.; Wang, J.; Jin, Q.; Yang, M.; Mao, D.; Kisailus, D.; Zhao, H.; Wang, D. Muftishelled TiO_2 Hollow Microspheres As Anodes with Superior Reversible Capacity for Lithium Ion Batteries. *Nano Lett.* **2014**, *14*, 6679−6684.

(6) Uchaker, E.; Cao, G. Mesocrystals As Electrode Materials for Lithium-ion Batteries. *Nano Today* **2014**, *9*, 499−524.

(7) Wang, H. Y.; Chen, J. Z.; Hy, S.; Yu, L. H.; Xu, Z. C.; Liu, B. High-Surface-Area Mesoporous TiO_2 Microspheres via One-Step Nanoparticle Self-Assembly for Enhanced Lithium-ion Storage. *Nanoscale* **2014**, *6*, 14926−14931.

(8) Wang, Z.; Zhou, L.; Lou, X. W. Metal Oxide Hollow Nanostructures for Lithium-ion Batteries. *Adv. Mater.* **2012**, *24*, 1903−1911.

(9) Zhang, G.; Wu, H. B.; Song, T.; Paik, U.; Lou, X. W. TiO_2 Hollow Spheres Composed of Highly Crystalline Nanocrystals Exhibit Superior Lithium Storage Properties. *Angew. Chem., Int. Ed.* **2014**, *53*, 12590−12593.

(10) Shao, Z.; Pan, X.; Chen, H.; Tao, L.; Wang, W.; Ding, Y.; Pan, B.; Yang, S.; Dai, S. Polymer Based Photocathodes for Panchromatic Tandem Dye-Sensitized Solar Cells. *Energy Environ. Sci.* **2014**, *7*, 2647−2651.

(11) Lei, B.-X.; Zhang, P.; Qiao, H.-K.; Zheng, X.-F.; Hu, Y.-S.; Huang, G.-L.; Sun, W.; Sun, Z.-F.; Zhang, X.-X. A Facile Template-Free Route for Synthesis of Anatase TiO_2 Hollow Spheres for Dye-Sensitized Solar Cells. *Electrochim. Acta* **2014**, *143*, 129−134.

(12) Rui, Y.; Li, Y.; Zhang, Q.; Wang, H. Facile Synthesis of Rutile TiO_2 Nanorod Microspheres for Enhancing Light-Harvesting of Dye-Sensitized Solar Cells. *CrystEngComm* **2013**, *15*, 1651−1656.

(13) Heiniger, L.-P.; Giordano, F.; Moehl, T.; Graetzel, M. Mesoporous TiO_2 Beads Offer Improved Mass Transport for Cobalt-Based Redox Couples Leading to High Efficiency Dye-Sensitized Solar Cells. *Adv. Energy Mater.* **2014**, *4*, 1400168-1−1400168-10.

(14) Lin, J.; Peng, Y.; Pascoe, A. R.; Huang, F.; Cheng, Y.-B.; Heo, Y.-U.; Nattestad, A.; Seung, W.; Kim, S. K.; Yoon, H. J.; Kim, S.-W.; Yamauchi, Y.; Dou, S. X.; Kim, J. H. A Bi-Layer TiO_2 Photoanode for Highly Durable, Flexible Dye-Sensitized Solar Cells. *J. Mater. Chem. A* **2015**, *3*, 4679−4686.

(15) Liu, Q.; Sun, Z.; Dou, Y.; Kim, J. H.; Dou, S. X. Two-Step Self-Assembly of Hierarchically-Ordered Nanostructures. *J. Mater. Chem. A* **2015**, *3*, 11688−11699.

(16) Lin, J.; Heo, Y.-U.; Nattestad, A.; Shahabuddin, M.; Yamauchi, Y.; Kim, J. H. N719- and D149-Sensitized 3D Hierarchical Rutile TiO_2 Solar Cells - A Comparative Study. *Phys. Chem. Chem. Phys.* **2015**, *17*, 7208−7213.

(17) Kim, J.; Koh, J. K.; Kim, B.; Kim, J. H.; Kim, E. Nanopatterning of Mesoporous Inorganic Oxide Films for Efficient Light Harvesting of Dye-Sensitized Solar Cells. *Angew. Chem., Int. Ed.* **2012**, *51*, 6864−6869.

(18) Koh, J. K.; Kim, J.; Kim, B.; Kim, J. H.; Kim, E. Highly Efficient, Iodine-Free Dye-Sensitized Solar Cells with Solid-State Synthesis of Conducting Polymers. *Adv. Mater.* **2011**, *23*, 1641−1646.

(19) Docampo, P.; Guldin, S.; Steiner, U.; Snaith, H. J. Charge Transport Limitations in Self-Assembled TiO_2 Photoanodes for Dye-Sensitized Solar Cells. *J. Phys. Chem. Lett.* **2013**, *4*, 698−703.

(20) Ding, Y.; Mo, L. E.; Tao, L.; Ma, Y. M.; Hu, L. H.; Huang, Y.; Fang, X. Q.; Yao, J. X.; Xi, X. W.; Dai, S. Y. TiO_2 Nanocrystalline Layer As A Bridge Linking TiO_2 Sub-Microspheres Layer and Substrates for High-Efficiency Dye-Sensitized Solar Cells. *J. Power Sources* **2014**, *272*, 1046−1052.

(21) Roh, D. K.; Chi, W. S.; Jeon, H.; Kim, S. J.; Kim, J. H. High Efficiency Solid-State Dye-Sensitized Solar Cells Assembled with Hierarchical Anatase Pine Tree-like TiO_2 Nanotubes. *Adv. Funct. Mater.* **2014**, *24*, 379−386.

(22) Lee, K.; Kirchgeorg, R.; Schmuki, P. Role of Transparent Electrodes for High Efficiency TiO_2 Nanotube Based Dye-Sensitized Solar Cells. *J. Phys. Chem. C* **2014**, *118*, 16562−16566.

DOI: 10.1021/acsami.5b06556
ACS Appl. Mater. Interfaces 2015, 7, 22277−22283

(23) Lin, J.; Guo, M.; Yip, C. T.; Lu, W.; Zhang, G.; Liu, X.; Zhou, L.; Chen, X.; Huang, H. High Temperature Crystallization of Free-Standing Anatase TiO_2 Nanotube Membranes for High Efficiency Dye-Sensitized Solar Cells. *Adv. Funct. Mater.* **2013**, *23*, 5952−5960.
(24) Wu, W.-Q.; Xu, Y.-F.; Rao, H.-S.; Su, C.-Y.; Kuang, D.-B. Multistack Integration of Three-Dimensional Hyperbranched Anatase Titania Architectures for High-Efficiency Dye-Sensitized Solar Cells. *J. Am. Chem. Soc.* **2014**, *136*, 6437−6445.
(25) Feng, X.; Shankar, K.; Varghese, O. K.; Paulose, M.; Latempa, T. J.; Grimes, C. A. Vertically Aligned Single Crystal TiO_2 Nanowire Arrays Grown Directly on Transparent Conducting Oxide Coated Glass: Synthesis Details and Applications. *Nano Lett.* **2008**, *8*, 3781−3786.
(26) Chen, Y.; Huang, F.; Chen, D.; Cao, L.; Zhang, X. L.; Caruso, R. A.; Cheng, Y.-B. Effect of Mesoporous TiO_2 Bead Diameter in Working Electrodes on the Efficiency of Dye-Sensitized Solar Cells. *ChemSusChem* **2011**, *4*, 1498−1503.
(27) Huang, F.; Chen, D.; Zhang, X. L.; Caruso, R. A.; Cheng, Y.-B. Dual-Function Scattering Layer of Submicrometer-Sized Mesoporous TiO_2 Beads for High-Efficiency Dye-Sensitized Solar Cells. *Adv. Funct. Mater.* **2010**, *20*, 1301−1305.
(28) Sauvage, F.; Chen, D.; Comte, P.; Huang, F.; Heiniger, L.-P.; Cheng, Y.-B.; Caruso, R. A.; Graetzel, M. Dye-Sensitized Solar Cells Employing a Single Film of Mesoporous TiO_2 Beads Achieve Power Conversion Efficiencies Over 10%. *ACS Nano* **2010**, *4*, 4420−4425.
(29) Gao, M. M.; Peh, C. K. N.; Pan, Y. L.; Xu, Q. H.; Ho, G. W. Fine Structural Tuning of Whereabout and Clustering of Metal-Metal Oxide Heterostructure for Optimal Photocatalytic Enhancement and Stability. *Nanoscale* **2014**, *6*, 12655−12664.
(30) Chandiran, A. K.; Comte, P.; Humphry-Baker, R.; Kessler, F.; Yi, C.; Nazeeruddin, M. K.; Grätzel, M. Evaluating the Critical Thickness of TiO_2 Layer on Insulating Mesoporous Templates for Efficient Current Collection in Dye-Sensitized Solar Cells. *Adv. Funct. Mater.* **2013**, *23*, 2775−2781.
(31) Hwang, S. H.; Yun, J.; Jang, J. Multi-Shell Porous TiO_2 Hollow Nanoparticles for Enhanced Light Harvesting in Dye-sensitized Solar Cells. *Adv. Funct. Mater.* **2014**, *24*, 7619−7626.
(32) Koo, H.-J.; Kim, Y. J.; Lee, Y. H.; Lee, W. I.; Kim, K.; Park, N.-G. Nano-Embossed Hollow Spherical TiO_2 As Bifunctional Material for High-Efficiency Dye-Sensitized Solar Cells. *Adv. Mater.* **2008**, *20*, 195−199.
(33) Kopidakis, N.; Neale, N. R.; Zhu, K.; van de Lagemaat, J.; Frank, A. J. Spatial Location of Transport-Limiting Traps in TiO_2 Nanoparticle Films in Dye-Sensitized Solar Cells. *Appl. Phys. Lett.* **2005**, *87*, 202106-1−202106-3.
(34) Liu, B.; Liu, L. M.; Lang, X. F.; Wang, H. Y.; Lou, X. W.; Aydil, E. S. Doping High-Surface-Area Mesoporous TiO_2 Microspheres with Carbonate for Visible Light Hydrogen Production. *Energy Environ. Sci.* **2014**, *7*, 2592−2597.
(35) Nakade, S.; Matsuda, M.; Kambe, S.; Saito, Y.; Kitamura, T.; Sakata, T.; Wada, Y.; Mori, H.; Yanagida, S. Dependence of TiO_2 Nanoparticle Preparation Methods and Annealing Temperature on the Efficiency of Dye-Sensitized Solar Cells. *J. Phys. Chem. B* **2002**, *106*, 10004−10010.
(36) Nakade, S.; Saito, Y.; Kubo, W.; Kitamura, T.; Wada, Y.; Yanagida, S. Influence of TiO_2 Nanoparticle Size on Electron Diffusion and Recombination in Dye-Sensitized TiO_2 Solar Cells. *J. Phys. Chem. B* **2003**, *107*, 8607−8611.
(37) Lee, S.-W.; Ahn, K.-S.; Zhu, K.; Neale, N. R.; Frank, A. J. Effects of $TiCl_4$ Treatment of Nanoporous TiO_2 Films on Morphology, Light Harvesting, and Charge-Carrier Dynamics in Dye-Sensitized Solar Cells. *J. Phys. Chem. C* **2012**, *116*, 21285−21290.
(38) Cui, Y.; Zhang, L.; Lv, K.; Zhou, G.; Wang, Z.-S. Low Temperature Preparation of TiO_2 Nanoparticle Chains without Hydrothermal Treatment for Highly Efficient Dye-Sensitized Solar Cells. *J. Mater. Chem. A* **2015**, *3*, 4477−4483.
(39) Wu, W.-Q.; Xu, Y.-F.; Rao, H.-S.; Su, C.-Y.; Kuang, D.-B. Trilayered Photoanode of TiO_2 Nanoparticles on a 1D-3D Nanostructured TiO_2-Grown Flexible Ti Substrate for High-Efficiency (9.1%) Dye-Sensitized Solar Cells with Unprecedentedly High Photocurrent Density. *J. Phys. Chem. C* **2014**, *118*, 16426−16432.
(40) Li, Z.-Q.; Que, Y.-P.; Mo, L.-E.; Chen, W.-C.; Ding, Y.; Ma, Y.-M.; Jiang, L.; Hu, L.-H.; Dai, S.-Y. One-Pot Synthesis of Mesoporous TiO_2 Microspheres and Its Application for High-Efficiency Dye-Sensitized Solar Cells. *ACS Appl. Mater. Interfaces* **2015**, *7*, 10928−10934.
(41) Lin, J.; Heo, Y.-U.; Nattestad, A.; Yamauchi, Y.; Dou, S. X.; Kim, J. H. Mesoporous Hierarchical Anatase for Dye-sensitized Solar Cells Achieving Over 10% Conversion Efficiency. *Electrochim. Acta* **2015**, *153*, 393−398.
(42) Tian, J.; Uchaker, E.; Zhang, Q.; Cao, G. Hierarchically Structured ZnO Nanorods-Nanosheets for Improved Quantum-Dot-Sensitized Solar Cells. *ACS Appl. Mater. Interfaces* **2014**, *6*, 4466−4472.
(43) Dong, Z.; Ren, H.; Hessel, C. M.; Wang, J.; Yu, R.; Jin, Q.; Yang, M.; Hu, Z.; Chen, Y.; Tang, Z.; Zhao, H.; Wang, D. Quintuple-Shelled SnO_2 Hollow Microspheres with Superior Light Scattering for High-Performance Dye Sensitized Solar Cells. *Adv. Mater.* **2014**, *26*, 905−909.
(44) Chen, D. H.; Huang, F. Z.; Cheng, Y. B.; Caruso, R. A. Mesoporous Anatase TiO_2 Beads with High Surface Areas and Controllable Pore Sizes: A Superior Candidate for High-Performance Dye-Sensitized Solar Cells. *Adv. Mater.* **2009**, *21*, 2206−2210.
(45) Chen, Y.; Huang, F.; Xiang, W.; Chen, D.; Cao, L.; Spiccia, L.; Caruso, R. A.; Cheng, Y.-B. Effect of TiO_2 Microbead Pore Size on the Performance of DSSCs with A Cobalt Based Electrolyte. *Nanoscale* **2014**, *6*, 13787−13794.
(46) Yue, G.; Zhang, X. a.; Wang, L.; Tan, F.; Wu, J.; Jiang, Q.; Lin, J.; Huang, M.; Lan, Z. Highly Efficient and Stable Dye-Sensitized Solar Cells Based on Nanographite/Polypyrrole Counter Electrode. *Electrochim. Acta* **2014**, *129*, 229−236.
(47) Yue, G.; Tan, F.; Li, F.; Chen, C.; Zhang, W.; Wu, J.; Li, Q. Enhanced Performance of Flexible Dye-Sensitized Solar Cell Based on Nickel Sulfide/Polyaniline/Titanium Counter Electrode. *Electrochim. Acta* **2014**, *149*, 117−125.
(48) Chen, H.; Kou, D.; Chang, Z.; Zhou, W.; Zhou, Z.; Wu, S. Effect of Crystallization of $Cu_2ZnSnS_xSe_{4-x}$ Counter Electrode on the Performance for Efficient Dye-Sensitized Solar Cells. *ACS Appl. Mater. Interfaces* **2014**, *6*, 20664−20669.
(49) Chi, Y.; Wu, K.-L.; Wei, T.-C. Ruthenium and Osmium Complexes That Bear Functional Azolate Chelates for Dye-Sensitized Solar Cells. *Chem. - Asian J.* **2015**, *10*, 1098−1115.
(50) Gao, F.; Wang, Y.; Shi, D.; Zhang, J.; Wang, M.; Jing, X.; Humphry-Baker, R.; Wang, P.; Zakeeruddin, S. M.; Graetzel, M. Enhance the Optical Absorptivity of Nanocrystalline TiO_2 Film with High Molar Extinction Coefficient Ruthenium Sensitizers for High Performance Dye-Sensitized Solar Cells. *J. Am. Chem. Soc.* **2008**, *130*, 10720−10728.
(51) Yella, A.; Lee, H. W.; Tsao, H. N.; Yi, C. Y.; Chandiran, A. K. Porphyrin-Sensitized Solar Cells with Cobalt (II/III)-Based Redox Electrolyte Exceed 12% Efficiency. *Science* **2011**, *334*, 629−634.
(52) Zhu, F.; Wu, D.; Li, Q.; Dong, H.; Li, J.; Jiang, K.; Xu, D. Hierarchical TiO_2 Microspheres: Synthesis, Structural Control and Their Applications in Dye-Sensitized Solar Cells. *RSC Adv.* **2012**, *2*, 11629−11637.
(53) O'Regan, B. C.; Durrant, J. R.; Sommeling, P. M.; Bakker, N. J. Influence of the $TiCl_4$ Treatment on Nanocrystalline TiO_2 Films in Dye-Sensitized Solar Cells. 2. Charge Density, Band Edge Shifts, and Quantification of Recombination Losses at Short Circuit. *J. Phys. Chem. C* **2007**, *111*, 14001−14010.
(54) Yu, I. G.; Kim, Y. J.; Kim, H. J.; Lee, C.; Lee, W. I. Size-Dependent Light-Scattering Effects of Nanoporous TiO_2 Spheres in Dye-Sensitized Solar Cells. *J. Mater. Chem.* **2011**, *21*, 532−538.

DOI: 10.1021/acsami.5b06556
ACS Appl. Mater. Interfaces 2015, 7, 22277−22283